JACS
JOURNAL OF THE AMERICAN CHEMICAL SOCIETY

Article

pubs.acs.org/JACS

Bright Core–Shell Semiconductor Quantum Wires

Yi-Hsin Liu, Fudong Wang, Jessica Hoy, Virginia L. Wayman, Lindsey K. Steinberg, Richard A. Loomis,* and William E. Buhro*

Department of Chemistry, Washington University, Saint Louis, Missouri 63130-4899, United States

Supporting Information

ABSTRACT: Colloidal CdTe quantum wires are reported having ensemble photoluminescence efficiencies as high as 25% under low excitation-power densities. High photoluminescence efficiencies are achieved by formation of a monolayer CdS shell on the CdTe quantum wires. Like other semiconductor nanowires, the CdTe quantum wires may contain frequent wurtzite–zinc-blende structural alternations along their lengths. The present results demonstrate that the optical properties, emission-peak shape and photoluminescence efficiencies, are independent of the presence or absence of such structural alternations.

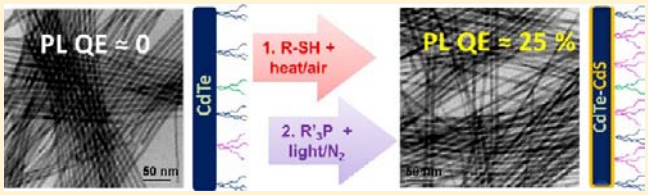

INTRODUCTION

Herein we show that colloidal CdTe quantum wires (QWs) having as-synthesized photoluminescence (PL) quantum efficiencies (QEs) of near zero are brightened to QEs of up to 25% by improved surface passivation. The enhancement is achieved by a surface-exchange process resulting in a monolayer CdS shell on the QWs. We demonstrate that the important exciton- or charge-trapping defects are not due to wurtzite–zinc-blende (W–ZB) structural alternations in the core of the QWs, but rather are on the QW surfaces. The results establish that the PL QEs of semiconductor QWs can be competitive with those of much shorter quantum rods.

Semiconductor nanowires and QWs are potentially capable of transporting energy and charge over distances, along the long axis of the wires. Such transport, if achieved efficiently, may enable nanowire devices for solar-energy conversion,[1] nanoelectronics,[2] and nanoscale light emission.[3] Efficient transport requires that wires be sufficiently free of trap-site defects such that excitons and charge carriers do not become trapped and their mobilities therefore impeded.

Unfortunately, the semiconductor QWs and nanowires accessible to date have possessed comparatively high trap-site populations, as revealed by low measured PL QEs.[4−12] Excitons and charge carriers that become trapped and therefore localized in defect sites have a low probability of radiative recombination at the band edge. Consequently, low band-edge PL QEs are indicative of defective wires, in which exciton and charge transport will be hindered.

The maximum PL QEs of 0.1–0.3% reported for ensembles of colloidal semiconductor QWs and nanowires are disappointingly low.[4−9] These values compare very unfavorably to the maximum values achieved for colloidal quantum dots (60–90%)[13−15] and quantum rods (20–30%).[16,17] The important trap-site defects in quantum dots and rods have been shown to be on the nanocrystal surfaces, and large enhancements in their band-edge PL QEs have been achieved over the past decade by optimization of surface passivation.[13−21]

The low PL QEs of QWs and nanowires have at least two potential origins. First, their long dimension provides an extremely large surface area for excitons and charge carriers to sample with excursions along the wire axis, greatly increasing their probability of finding surface trap sites. Thus, QWs and nanowires may have lower PL QEs than those of quantum dots and rods merely because they have much larger total surface areas. If so, efficient energy and charge transport in QWs and nanowires will require even better surface passivation than that in quantum dots and rods.

Internal, core defects in QWs and nanowires provide a second potential origin for their low PL efficiencies. Nearly all semiconductor nanowires and QWs grown by SLS, VLS, or related mechanisms contain frequent W–ZB structural alternations along their long axis. These alternations result in high populations of twinning boundaries and stacking faults, and an undulating energy landscape due to the varying W and ZB band offsets. As these types of defect are generally absent from quantum dots and rods, their possible role in generating internal trap-site defects in QWs and nanowires should be evaluated.

We report that a monolayer shell of CdS is formed on presynthesized CdTe QWs by surface adsorption of ethanethiol (EtSH) followed by oxidative-substitution and photochemical steps. The enhanced PL QE in the CdTe–CdS core–shell wires, currently maximized at 25%, is 2 orders of magnitude higher than has been reported for other semiconductor QW or nanowire specimens.[4−9] Comparison of core–shell QWs in which the CdTe cores contain frequent W–ZB alternations to those in which the cores are predominantly W reveals that the PL peak shape and QE are independent of these core structural

Received: September 5, 2012
Published: October 24, 2012

   dx.doi.org/10.1021/ja3088218 | J. Am. Chem. Soc. 2012, 134, 18797–18803

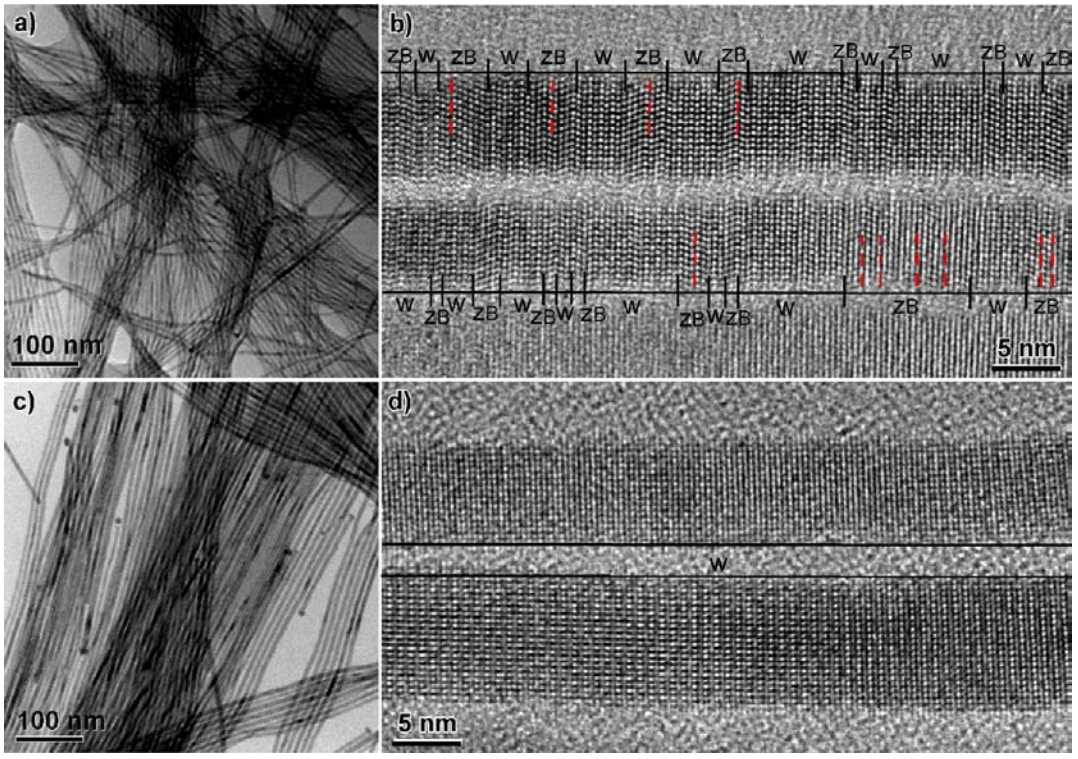

Figure 1. Representative TEM (a and c) and HRTEM (b and d) images of CdTe QWs. The QWs were grown from 6.5-nm Bi NPs using the ODPA protocol[12] (a and b) and from 10.3-nm Bi NPs using the OA-TDPA-DOPA protocol (c and d). Mean diameter (d) ± one standard deviation (σ) in the diameter distribution, expressed as a percentage of the mean diameter =5.5 nm ±16% (a and b), and 8.2 nm ±13% (c and d). HRTEM images of the QWs (b and d) were viewed in the zinc blende (ZB) [011] or wurtzite (W) [$2\bar{1}\bar{1}0$] zone normal to the growth axis of ZB [111] and W [0001]. The ZB and W segments are labeled as indicated. The red dashed lines denote twin boundaries or stacking faults.

aspects. Therefore, the important trap-site defects are predominantly on the surfaces of the CdTe QWs, and when they are properly passivated, the optical properties of the QWs become comparable to those of other semiconductor nanocrystals.

EXPERIMENTAL SECTION

Materials. Cadmium oxide (CdO, 99.99+%, Aldrich), tellurium granules (Te, −5 + 50 mesh, 99.99%, Aldrich), tri-*n*-octylphosphine (TOP, 90%, Aldrich), *n*-octadecylphosphonic acid (ODPA, >99%, PCI Synthesis), *n*-tetradecylphosphonic acid (TDPA, >99%, PCI Synthesis), oleic acid (OA, 90%, Aldrich), ethanethiol (EtSH, 97%, Aldrich), and 1-hexanethiol (95%, Aldrich) were used as received. Tri-*n*-octylphosphine oxide (TOPO, 90%, Aldrich) was either distilled[12] or recrystallized[22,23] before use. Bismuth (Bi) NP stock solutions (0.04 mmol Bi atoms g^{-1} solution)[8,24] and di-*n*-octylphosphinic acid (DOPA)[22,23] were synthesized using previously reported procedures. The tri-*n*-octylphosphine telluride (TOPTe) stock solution (0.025 mmol/g solution) was prepared by dissolving Te (0.051 g, 0.40 mmol) into TOP (15.8 g, 42.7 mmol) with stirring at room temperature in a N_2 (g)-filled glovebox. Toluene (CHROMASOLV for HPLC, Sigma-Aldrich) was distilled under N_2 (g) over Na/benzophenone ketyl, and referred to as dried toluene. All synthetic procedures for CdTe QWs described below were conducted under dry, O_2-free N_2 (g). Dried toluene (18.5 g) was added in a N_2 (g)-filled glovebox to the as-synthesized CdTe QWs before solidification. The CdTe-QW−toluene dispersion stored in this condition was stable over several years.

Synthesis of CdTe QWs Having Frequent W−ZB Alternations. The synthesis was adapted from a previously reported procedure,[12] referred to as the ODPA protocol. In a typical synthesis of 5.5-nm-diameter QWs, CdO (0.016 g, 0.12 mmol), ODPA (0.052 g, 0.16 mmol), and distilled TOPO (4.99 g, 12.9 mmol) were loaded into a Schlenk reaction tube. The 6.5-nm Bi nanoparticle stock solution (0.026 g, 0.001 mmol Bi) and TOPTe stock solution (1.25 g, 0.031 mmol) were combined in a vial, which was septum capped. The mixture of TOPTe and Bi NPs was then loaded into a syringe. The reaction tube was heated to 340 °C in a salt bath ($NaNO_3$/KNO_3, 46:54 by weight) to obtain a clear solution (~5 min), which was then switched to a 248 °C salt bath. After 2−3 min equilibration of the reaction mixture at 248 °C, the mixture of TOPTe and Bi NPs was quickly injected into the reaction tube. The amount of TOPTe (0.030 mmol) injected was measured as the difference between masses of the syringe before and after the injection. The reaction tube was withdrawn from the salt bath 5 min after the injection with a resulting brownish black solution.

Synthesis of CdTe QWs Having a Predominantly W Crystal Structure. The synthesis was referred to as the OA-TDPA-DOPA protocol. In a typical synthesis of 7.7-nm-diameter QWs, CdO (0.014 g, 0.11 mmol), OA (0.096 g, 0.34 mmol), TDPA (0.012 g, 0.043 mmol), DOPA (0.012 g, 0.041 mmol), and recrystallized TOPO (4.14 g, 10.7 mmol) were loaded into a Schlenk reaction tube. The 10.3-nm Bi nanoparticle stock solution (0.019 g, 0.00076 mmol Bi) and TOPTe stock solution (0.744 g, 0.0186 mmol) were combined in a vial, which was septum capped. The mixture of TOPTe and Bi NPs was then loaded into a syringe. The reaction tube was heated to 320 °C in a salt bath to obtain a clear solution (80 min), which was then switched to a 248 °C salt bath. After 2−3 min equilibration of the reaction mixture at 248 °C, the mixture of TOPTe and Bi NPs was quickly injected into the reaction tube. The amount of TOPTe (0.017 mmol) injected was measured as the difference between masses of the syringe before and after the injection. The reaction tube was withdrawn from the salt bath 5.5 min after the injection with a resulting brownish black solution.

PL Enhancement. This step was conducted in air, unless otherwise specified. An aliquot of the CdTe-QW−toluene suspension (~1.0 mL, ~0.001 mmol CdTe, assuming 100% conversion of the limiting reagent, TOPTe, into CdTe) and dried toluene (1.5 mL) were

dx.doi.org/10.1021/ja3088218 | J. Am. Chem. Soc. 2012, 134, 18797−18803

loaded into a cuvette or (borosilicate) test tube, which was capped and taken out of the glovebox. EtSH (1.5 mL, 21 mmol) (or 1-hexanethiol, 1.5 mL, 11 mmol, for the purpose of mass spectrometric analysis of the surface ligands on wires, see the Supporting Information for details) was injected via a syringe into the cuvette/tube with its enclosure open to the atmosphere for 1−2 s, and then the cuvette/tube was capped and further sealed with parafilm. The cuvette/tube was placed in a sand bath at 100 °C for 12−24 h (step 1), resulting in several flocculated, black QW aggregates suspended in the solution. The black aggregates were precipitated via centrifugation (benchtop centrifuge, 700*g*) and the supernatant was removed and discarded via a syringe. A proper amount of TOP was added to the cuvette/tube containing the QW precipitate to ensure the optical density of the QWs in the range of 0.02−0.1 absorbance at the excitation wavelength 585 nm (2.1 eV). (Loading of TOP can be conducted under either air or N_2.) The QW−TOP dispersion in a cuvette was placed at a 5-cm distance from a 100-W incandescent light source with a power intensity of 200 mW/cm^2 (step 2). The PL spectra of the QW−TOP dispersion were acquired at various time intervals to monitor the photoenhancement process.

RESULTS

Synthesis of W-ZB and W Core-Only CdTe QWs. The preparation of CdTe QWs having frequent W−ZB alternations was an adaptation of our previously published method.[12] Wire growth was catalyzed by 6.5-nm Bi nanoparticles. The important synthetic conditions employed were (1) the use of octadecylphosphonic acid to dissolve the CdO precursor, and (2) the use of distilled 90%-purity grade TOPO as the solvent, which is known to contain influential trace impurities.[22,23]

TEM images of the W−ZB QWs are shown in Figure 1a,b. The mean QW diameter measured from the images was 5.5 ± 0.9 nm, and the mean length was greater than 5 μm. The high-resolution (HR) TEM image in Figure 1b revealed the W−ZB alternations, which were found in all of the >50 wires examined.

The OA-TDPA-DOPA synthetic procedure was found empirically to provide CdTe QWs possessing predominantly W crystal structures. The altered synthetic parameters were the use of (1) oleic acid as the major acid to dissolve the CdO precursor; (2) purified TOPO as the solvent, with small amounts of DOPA and TDPA as purposeful additives; and (3) 10.3-nm Bi nanoparticles.[8,24] Control studies established that the size of the Bi nanoparticles or the diameter of the CdTe QWs were not correlated with the core crystal structure (W vs ZB). A slightly different Cd:Te precursor molar ratio of 6.5:1.0 was also employed here, as compared to a ratio of 4.0:1.0 for the preparation of the W−ZB QWs, but the significance of that small difference is unknown.

TEM images of the W-predominant QWs are shown in Figure 1c,d. The mean QW diameter measured from the images was 8.2 ± 1.1 nm, and the mean length was greater than 5 μm. The high-resolution image in Figure 1d showed smooth, extended W domains free of stacking faults and twinning boundaries, which were >50 nm in length. Such W-predominant structures were found in all 17 QWs examined in this specimen. Attempts to reproduce the synthetic conditions gave mixtures of 60−70% W-predominant QWs and 40−30% W−ZB QWs. Obviously, a structure-determining parameter is not yet fully controlled.

Shell Growth and PL Enhancement. The as-synthesized CdTe QWs, either W-predominant or W−ZB alternating, exhibited immeasurably low PL QEs below our detection capability (Figure 2a). Wires of both types were brightened by a two-step procedure. In the first step, EtSH was added to a toluene dispersion of as-synthesized QWs in the presence of air.

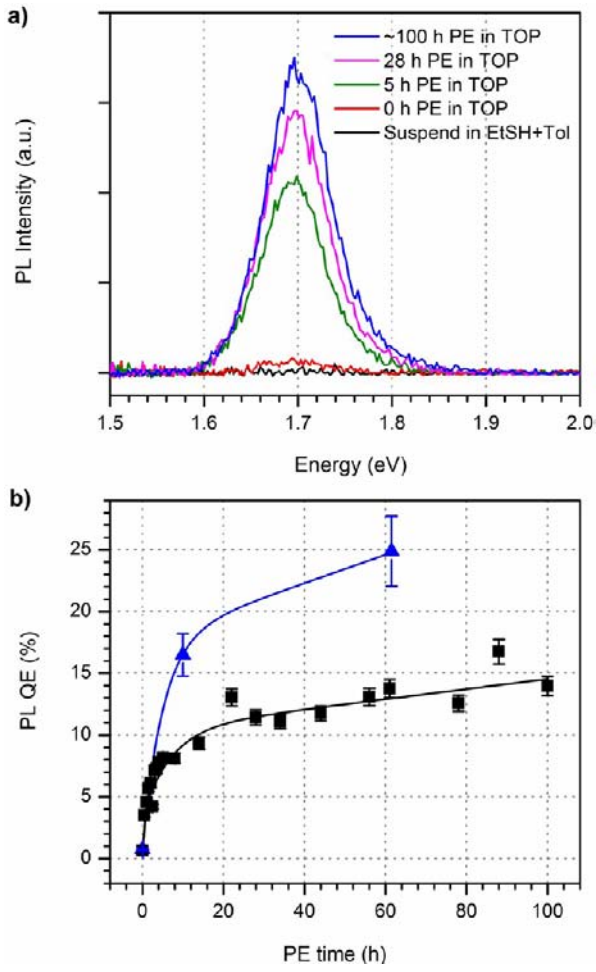

Figure 2. PL enhancement for CdTe QWs grown using the OA-TDPA-DOPA protocol. (a) PL spectra of CdTe QWs at different stages of PL enhancement: as-synthesized QWs suspended in EtSH and dried toluene (black); acquired during photoenhancing (step 2) in TOP at t = 0 (red), 5 (olive), 28 (magenta), and ~100 h (blue). The QWs were heated in EtSH and dried toluene for 12 h before photoenhancing. See the Experimental Section for details. The PL spectra were acquired at an excitation wavelength of 585 nm (2.1 eV) with a power density of 300 μW/cm^2 (3000 excitons photogenerated per wire per second). (b) PL QE as a function of photoenhancement (PE) time in TOP. The black squares are associated with the PL measurements for which some spectra are shown in (a). The blue triangles are data acquired from the same QW batch with the same PE conditions except using 23.3 h of heating in EtSH and dried toluene. The blue and black lines are the double and triple-exponential fits to guide the eye, respectively.

The specimen was then heated to 100 °C for 12−24 h. We show below that a monolayer CdS shell was formed on the QWs by a thermal process in this step, although the PL QEs were only marginally increased, and remained low (Figure 2a). When this shell-formation step was conducted under an N_2 atmosphere without purposeful introduction of air, the maximum PL QEs ultimately obtained were reduced by an order of magnitude.

In the second step, the QWs were redispersed in TOP and subjected to illumination by an incandescent lamp for up to 100 h. Spectroscopic monitoring during illumination established a steady increase in PL QE, which grew to a maximum of 15−25% in some specimens. In other specimens in which shell growth (step 1) was not optimal (due to insufficient air

dx.doi.org/10.1021/ja3088218 | J. Am. Chem. Soc. 2012, 134, 18797−18803

exposure), the PL QEs maximized in the range of 3−8%. This step-2 photoenhancement was partially reversible, in that PL QEs decreased slowly in the dark (absence of light). Control experiments confirmed the photoenhancement to be photochemical and not thermal in nature (Figure S1, Supporting Information). The QEs dropped dramatically after the QWs were precipitated by adding methanol and transferred to toluene. Exposure to air, water, or alcoholic solvents quickly bleached the PL intensity.

A combination of TEM, absorption, EDS, and mass-spectral data was used to confirm the formation of an epitaxial, monolayer CdS shell on the CdTe QWs. Figure 3 presents

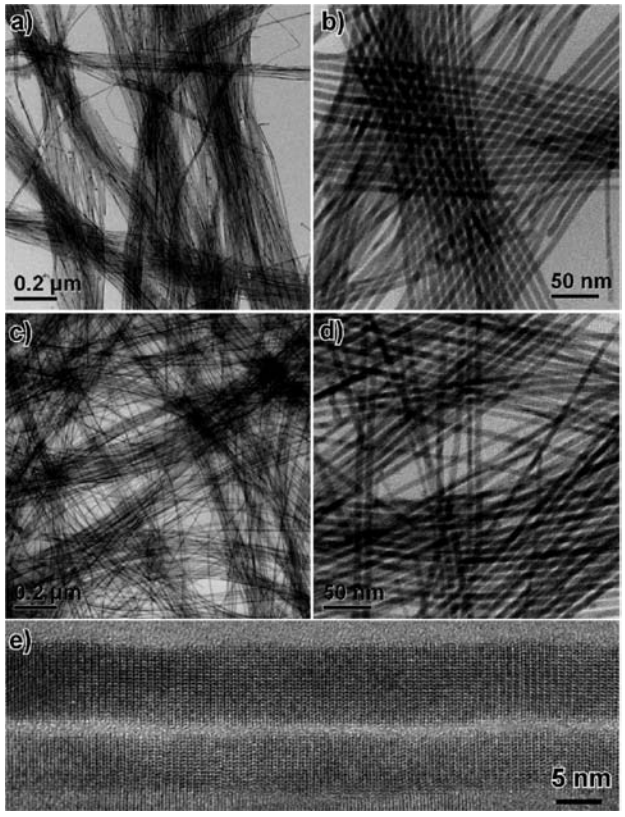

Figure 3. Representative TEM images of the as-synthesized CdTe QWs grown using the OA-TDPA-DOPA protocol (a and b) and the same QWs after photoenhancement in TOP (step 2, ∼100 h, c and d), referred to as CdTe−CdS core−shell QWs, and representative HRTEM image of the CdTe−CdS core−shell QWs (e). $d \pm \sigma$ = 7.7 nm ± 10% (a and b), and 7.5 nm ± 11% (c and d). The scale bars are 0.2 μm (c) and 50 nm (d), respectively.

TEM images of a QW specimen before and after CdS shell growth. The images showed that the initial mean QW diameter (7.7 ± 0.8 nm) apparently decreased slightly upon shell formation (7.5 ± 0.8 nm). The position of the first excitonic transition in the absorption spectrum was used to determine the effective core diameter in the core−shell QWs (Figure S2), which was so established to be 7.2 ± 0.8 nm. The resulting shell thickness obtained by difference (0.15 ± 0.6 nm) is close to $a/2$ = 0.21 nm in the CdS wurtzite unit cell. Because the long axis of the QWs was oriented along the wurtzite c axis, the value $a/2$ was used to estimate a CdS monolayer thickness in orthogonal directions, consistent with the dimensionality of shell formation. That the effective CdTe core diameter decreased upon shell formation suggested a substitution process in which surface Te atoms were replaced by S atoms to generate the CdS shell.

The mean core and shell thicknesses determined above were compared with those obtained from EDS data from the same core−shell QWs. EDS found the relative percentages to be Cd = 49.9 ± 1.0 mol %, Te = 45.9 ± 1.0 mol %, and S = 4.2 ± 1.0 mol % (Figure S3). These data and the mean QW diameter measured by TEM were used in a geometrical core−shell cylinder model to calculate the core and shell thicknesses (see the Supporting Information). The results established a core thickness of 7.2 ± 0.6 nm and a shell thickness of 0.15 ± 0.3 nm, confirming the determination above based on TEM and absorption data.

Mass-spectral results were used to distinguish between a CdS shell and a surface consisting of Cd−SEt ligation. The shell-formation procedure was repeated using 1-hexanethiol in place of EtSH, and was found to follow the same pathway for shell formation described above. (The procedures were not optimized to provide the same level of PL enhancements.) The surface ligation of the core−shell QWs was isolated by acid extraction and workup, and the liberated surface ligands were analyzed by mass spectrometry. DOPA and TOPO were detected, but no 1-hexanethiol-derived fragments or species were found (Figure S4). The results suggest that the alkyl groups were cleaved from the thiolate ligands during the first step, forming a CdS shell.

The CdS shells were shown to be epitaxial by HRTEM. Figure 3e contains high-resolution lattice images of two CdTe−CdS core−shell wires. Notably, the shells were not distinguishable from the cores. A comparison of Figures 3e and 1d showed the surfaces to be comparably smooth. The wurtzite structure in Figure 3e extended continuously through the cores and the shells without an evident interface, dislocations, or discontinuities, confirming the epitaxial core−shell relationship.

Comparison of PL Peak Profiles. The PL emission features obtained from ensembles of W-predominant, W−ZB, and a mixture of W-predominant and W−ZB CdTe QWs are compared in Figure 4. These nearly symmetrical peaks had similar peak centers and half widths. The slight blue shift and slightly broader peak for the W−ZB specimen were due to its smaller mean diameter and slightly broader diameter distribution (see the Figure 1 caption). The strong similarity of the PL peak profiles in specimens having different QW core structures (W vs W−ZB) but exhibiting comparatively high PL QEs suggested that the PL properties of the QWs were not strongly dependent on the core structure.

In samples having lower PL QEs (3−8%), the PL spectra often exhibited either or both high-energy and low-energy shoulders on the band-edge feature. Figure 5a contains the ensemble PL spectrum from such a W−ZB sample. Both high- and low-energy shoulders are evident. We surmise that these shoulder features are less pronounced or not observed in the spectra of the better-passivated specimens in Figure 4 because of a relative enhancement of the band-edge PL in those specimens.

Figure 5 also contains single-wire PL spectra and images for individual QWs from the ensemble. The peak centers and half widths of these emission features are very similar to one another, and to the ensemble spectrum, indicating a high degree of diameter uniformity in the sample. The PL images show emission, although not fully uniform, along the lengths of the QWs. Thus, the shell passivation extends along the QWs, and is not separated into isolated domains.

dx.doi.org/10.1021/ja3088218 | J. Am. Chem. Soc. 2012, 134, 18797−18803

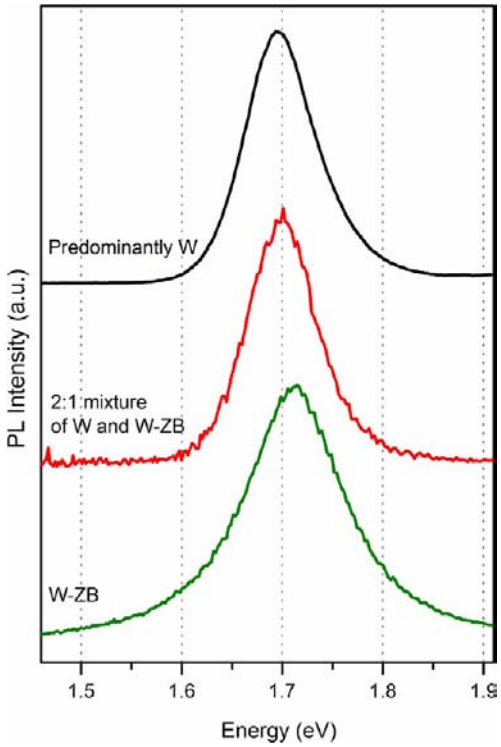

Figure 4. Ensemble PL spectral shapes for CdTe–CdS core–shell QWs having predominantly W (grown using the OA-TDPA-DOPA protocol), a 2:1 mixture of W and W–ZB alternations (grown using the OA-TDPA-DOPA protocol), and frequent W–ZB alternations (grown using the ODPA protocol). The corresponding PL peaks (and fwhms) are 1.694 (0.082), 1.701 (0.074), and 1.715 eV (0.113 eV), respectively. The ensemble PL QEs were 8–15%. The PL spectra were not acquired using identical parameters.

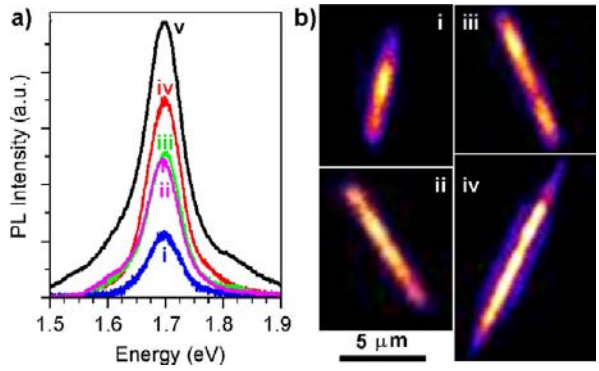

Figure 5. PL spectra of single CdTe–CdS core–shell QWs (a: i–iv) and their corresponding PL images (b), acquired at an excitation wavelength of 488 nm (2.54 eV). (v) is the ensemble PL spectrum of the QWs acquired at an excitation wavelength of 510 nm (2.43 eV). The ensemble PL QEs were ~5%.

Another set of single-wire PL spectra and images obtained from W–ZB QWs are given in Figure 6. The spectra indicate that individual wires can show band-edge emission only, or have low- and/or high-energy shoulders. Even so, the PL images resemble one another and those in Figure 5.

DISCUSSION

The results above establish that CdS-shell formation (step 1) is a thermal process that substitutes surface Te^{2-} for S^{2-} ions, requires air (thus O_2 or H_2O), and produces a monolayer shell.

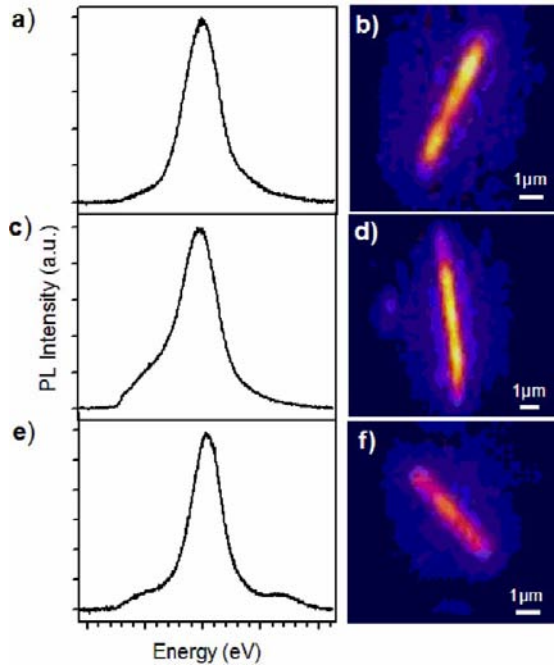

Figure 6. PL spectra of single CdTe–CdS core–shell QWs (left panel) and their corresponding PL images (right panel), acquired at an excitation wavelength of 488 nm (2.54 eV). These samples are from the same synthetic batch as those in Figure 5, but the shell formation and photoenhancement were conducted less ideally. The ensemble PL QEs were <1%.

Kotov and co-workers have reported oxidative-substitution chemistry that converts CdTe nanoparticles to CdS nanoparticles by the overall reaction in eq 1.[25] We propose this reaction to occur here, and to be responsible for CdS-shell formation. As the surface Te^{2-} ions are most accessible to the surface-exchange process, the reaction terminates here at one monolayer, producing smooth and uniform core–shell QWs (Figure 3c–e).

$$4Te^{2-} + O_2 + 4HSR \rightarrow 4Te + 2R_2 + 4S^{2-} + 2H_2O \quad (1)$$

Kuno and co-workers,[26] Mews and co-workers,[5] and others[27,28] have studied shell growth on colloidal II–VI QWs. These efforts have resulted in thick, roughened, nonepitaxial shells. The PL QEs are at best only minimally increased in such core–shell wires (for example, the PL QE in CdSe–CdS QWs is reported to be 0.46%[5]).

The roughened, discontinuous shells observed in the prior studies are the result of misfit strain, which is accommodated in core–shell quantum dots because of the relatively small interfacial area and thus relatively low misfit-strain energy.[29] However, QWs have an extended axial dimension, and considerable misfit strain accumulates along the long dimension of the core–shell interface. Experimental and theoretical studies[30−34] have shown that such misfit strain in QWs and nanowires is relaxed in part by the formation of sinusoidal[35] or helical[34] surface modulations. Shell breakage or shell islanding occurs when these modulations become sufficiently extreme.

In contrast, the CdS shells formed in the present study are smooth and epitaxial, resulting in a type-I heterostructure that dramatically increases the PL QEs of the CdTe QWs. The near-uniform PL emission observed along the lengths of the QWs (Figure 5b) indicates continuous, near-ideal shell formation.

dx.doi.org/10.1021/ja3088218 | J. Am. Chem. Soc. 2012, 134, 18797–18803

Although the CdTe−CdS lattice mismatch is large (≈11%), the success achieved likely results from the monolayer thinness of the shells, and the low temperature at which the oxidative-substitution process forming the shells was conducted. Hollingsworth and co-workers have previously shown that shell formation by surface-cation exchange produces large enhancements of PL QE in PbSe quantum dots.[36]

To our knowledge, PL QEs in the range of 15−25% are the highest that have been achieved on an ensemble of colloidal QWs under low excitation fluence. We previously reported whole-wire blinking in a small fraction of single CdSe QWs in sample having low ensemble PL QEs of ≈0.2%.[6] The PL QEs in these single CdSe QWs in their bright, on states were as high as 20%. However, these bright states were achieved only under high excitation fluences in the range of 7−100 W/cm^2. We argued that after the surface traps on the CdSe QWs were filled with photogenerated carriers or excitons, radiative recombination of subsequently generated excitons was enabled, accounting for the high single-wire PL QEs under high excitation power densities.[37] Under low excitation power densities, the surface traps remained largely empty, and interaction of excitons with these traps made nonradiative recombination the dominant exciton-relaxation pathway. Kuno and co-workers have also reported that the PL QEs in single colloidal QWs increase under increasing excitation intensities of up to 3000 W/cm^2, reaching values as high as 5−20%.[38,39]

In contrast, the excitation fluences in the ensemble measurements reported here were only 0.3 mW/cm^2, which are 4−5 orders of magnitude lower than those employed in the single-QW studies discussed above. Consequently, the high PL QEs reported here are not achieved by the temporal photofilling of surface traps. Instead, they are achieved from the elimination of surface traps by the type-I core−shell interface.

The ability of this shell-formation process to brighten both W−ZB and W-predominant CdTe QWs, and the similarity of the PL peak profiles obtained from the brightened specimens of each, strongly suggest that stacking faults and twinning boundaries (abundantly present in the W−ZB QWs) do not interact significantly with photogenerated excitons. These core defects apparently do not function as exciton or carrier trap sites. A related observation by Mews and co-workers is that the lengths of the alternating W and ZB domains are too short to confine (localize) carriers in the cores along the axial dimension of QWs.[40] That shell formation is capable of removing trap sites is consistent with the largest population of traps being on the surfaces of the CdTe core-only QWs, as in colloidal semiconductor quantum dots and rods.

CONCLUSION

The results reported here show that pseudocylindrical QWs may exhibit PL QEs of up to 25%, which are comparable to those of other nanocrystals having extended dimensions. As noted previously, the optimized PL QEs in quantum rods are in the range of 20−30%.[16,17] The reported PL QEs in quantum belts and platelets (nanoribbons and nanoplatelets) are in the range of 30−50%.[41−45] We have proposed that such flat colloidal nanocrystals acquire very effective self-assembled-monolayer passivation of their broad surfaces from the growth pathway,[46] and that trap-site defects are largely confined to the thin belt or platelet edges.[41]

Pseudocylindrical QWs likely expose additional facets and edges than do flat colloidal nanocrystals, and possess much larger surface areas than do quantum dots and rods. Thus, achieving effective surface passivation for wires should be more challenging, and has proven to be so. We have now shown that the growth of a Type-I interface by a substitutive monolayer shell formation achieves such effective passivation. New challenges are to extend this approach to other QW systems, and to determine if the core−shell interfaces, and thus the optimized optical properties, remain stable over time.

ASSOCIATED CONTENT

Supporting Information

Methods for optical spectroscopy, isolation and purification of QWs, TEM and HRTEM analyses, and mass spectrometry, and methods to establish the step-2 photochemical process and to identify the CdS shell on CdTe QWs. This material is available free of charge via the Internet at http://pubs.acs.org.

AUTHOR INFORMATION

Corresponding Author

buhro@wustl.edu; loomis@wustl.edu.

Notes

The authors declare no competing financial interest.

ACKNOWLEDGMENTS

This work was supported by NSF (CHE-1012898 for W.E.B. and DMR-0906966 for R.A.L.). Mass spectrometry was conducted by Ms. Jing Li and Dr. Weidong Cui of the Washington University Mass Spectrometry Resource, an NIH Research Resource (Grant No. P41RR0954).

REFERENCES

(1) Law, M. G., L.; Johnson, J. C.; Saykally, R.; Yang, P. *Nat. Mater.* **2005**, *415*, 617−620.
(2) Duan, X. H., Y.; Cui, Y.; Wang, J.; Lieber, C. M. *Nature* **2001**, *409*, 66−69.
(3) Gudikson, M. S. L., L. J.; Wang, J.; Smith, D. C.; Lieber, C. M. *Nature* **2002**, *415*, 617−620.
(4) Protasenko, V. V.; Hull, K. L.; Kuno, M. *Adv. Mater.* **2005**, *17*, 2942−2949.
(5) Li, Z.; Ma, X. D.; Sun, Q. A.; Wang, Z.; Liu, J. A.; Zhu, Z. H.; Qiao, S. Z.; Smith, S. C.; Lu, G. Q.; Mews, A. *Eur. J. Inorg. Chem.* **2010**, 4325−4331.
(6) Glennon, J. J.; Tang, R.; Buhro, W. E.; Loomis, R. A. *Nano Lett.* **2007**, *7*, 3290−3295.
(7) Kuno, M. *Phys. Chem. Chem. Phys.* **2008**, *10*, 620−639.
(8) Wang, F. D.; Buhro, W. E. *Small* **2010**, *6*, 573−581.
(9) Protasenko, V.; Gordeyev, S.; Kuno, M. *J. Am. Chem. Soc.* **2007**, *129*, 13160−13171.
(10) Wang, F.; Yu, H.; Li, J.; Hang, Q.; Zemlyanov, D.; Gibbons, P. C.; Wang, L. W.; Janes, D. B.; Buhro, W. E. *J. Am. Chem. Soc.* **2007**, *129*, 14327−14335.
(11) Yu, H.; Li, J. B.; Loomis, R. A.; Gibbons, P. C.; Wang, L. W.; Buhro, W. E. *J. Am. Chem. Soc.* **2003**, *125*, 16168−16169.
(12) Sun, J.; Wang, L. W.; Buhro, W. E. *J. Am. Chem. Soc.* **2008**, *130*, 7997−8005.
(13) Qu, L. H.; Peng, X. G. *J. Am. Chem. Soc.* **2002**, *124*, 2049−2055.
(14) Xie, R. G.; Kolb, U.; Li, J. X.; Basche, T.; Mews, A. *J. Am. Chem. Soc.* **2005**, *127*, 7480−7488.
(15) Reiss, P.; Bleuse, J.; Pron, A. *Nano Lett.* **2002**, *2*, 781−784.
(16) Mokari, T.; Banin, U. *Chem. Mater.* **2003**, *15*, 3955−3960.
(17) Manna, L.; Scher, E. C.; Li, L. S.; Alivisatos, A. P. *J. Am. Chem. Soc.* **2002**, *124*, 7136−7145.
(18) Dabbousi, B. O.; RodriguezViejo, J.; Mikulec, F. V.; Heine, J. R.; Mattoussi, H.; Ober, R.; Jensen, K. F.; Bawendi, M. G. *J. Phys. Chem. B* **1997**, *101*, 9463−9475.

(19) Li, J. J.; Wang, Y. A.; Guo, W. Z.; Keay, J. C.; Mishima, T. D.; Johnson, M. B.; Peng, X. G. *J. Am. Chem. Soc.* **2003**, *125*, 12567−12575.
(20) Peng, X. G.; Schlamp, M. C.; Kadavanich, A. V.; Alivisatos, A. P. *J. Am. Chem. Soc.* **1997**, *119*, 7019−7029.
(21) Talapin, D. V.; Rogach, A. L.; Shevchenko, E. V.; Kornowski, A.; Haase, M.; Weller, H. *J. Am. Chem. Soc.* **2002**, *124*, 5782−5790.
(22) Wang, F.; Tang, R.; Kao, J. L. F.; Dingman, S. D.; Buhro, W. E. *J. Am. Chem. Soc.* **2009**, *131*, 4983−4994.
(23) Wang, F. D.; Tang, R.; Buhro, W. E. *Nano Lett.* **2008**, *8*, 3521−3524.
(24) Wang, F. D.; Tang, R.; Yu, H.; Gibbons, P. C.; Buhro, W. E. *Chem. Mater.* **2008**, *20*, 3656−3662.
(25) Tang, Z. Y.; Wang, Y.; Shanbhag, S.; Kotov, N. A. *J. Am. Chem. Soc.* **2006**, *128*, 7036−7042.
(26) Goebl, J. A.; Black, R. W.; Puthussery, J.; Giblin, J.; Kosel, T. H.; Kuno, M. *J. Am. Chem. Soc.* **2008**, *130*, 14822−14833.
(27) Jiang, F. L., J.; Li, Y.; Fan, L.; Ding, Y.; Li, Y. *Adv. Funct. Mater.* **2012**, *22*, 2402−2411.
(28) Liu, S.; Zhang, W. H.; Li, C. *J. Cryst. Growth* **2011**, *336*, 94−100.
(29) Reiss, P.; Protiere, M.; Li, L. *Small* **2009**, *5*, 154−168.
(30) Trammell, T. E.; Zhang, X.; Li, Y. L.; Chen, L. Q.; Dickey, E. C. *J. Cryst. Growth* **2008**, *310*, 3084−3092.
(31) Li, X. L.; Yang, G. W. *J. Phys. Chem. C* **2009**, *113*, 12402−12406.
(32) Goldthorpe, I. A.; Marshall, A. F.; McIntyre, P. C. *Nano Lett.* **2009**, *9*, 3715−3719.
(33) Hu, S.; Kawamura, Y.; Huang, K. C. Y.; Li, Y. Y.; Marshall, A. F.; Itoh, K. M.; Brongersma, M. L.; McIntyre, P. C. *Nano Lett.* **2012**, *12*, 1385−1391.
(34) Wang, H. L.; Upmanyu, M.; Ciobanu, C. V. *Nano Lett.* **2008**, *8*, 4305−4311.
(35) Schmidt, V.; McIntyre, P. C.; Gosele, U. *Phys. Rev. B* **2008**, *77*, 235302.
(36) Pietryga, J. M.; Werder, D. J.; Williams, D. J.; Casson, J. L.; Schaller, R. D.; Klimov, V. I.; Hollingsworth, J. A. *J. Am. Chem. Soc.* **2008**, *130*, 4879−4885.
(37) Glennon, J. J.; Buhro, W. E.; Loomis, R. A. *J. Phys. Chem. C* **2008**, *112*, 4813−4817.
(38) Vietmeyer, F.; McDonald, M. P.; Kuno, M. *J. Phys. Chem. C* **2012**, *116*, 12379−12396.
(39) Giblin, J.; Vietmeyer, F.; McDonald, M. P.; Kuno, M. *Nano Lett.* **2011**, *11*, 3307−3311.
(40) Myalitsin, A.; Strelow, C.; Wang, Z.; Li, Z.; Kipp, T.; Mews, A. *ACS Nano* **2011**, *5*, 7920−7927.
(41) Liu, Y. H.; Wayman, V. L.; Gibbons, P. C.; Loomis, R. A.; Buhro, W. E. *Nano Lett.* **2010**, *10*, 352−357.
(42) Ithurria, S.; Tessier, M. D.; Mahler, B.; Lobo, R.; Dubertret, B.; Efros, A. *Nat. Mater.* **2011**, *10*, 936−941.
(43) Ithurria, S.; Bousquet, G.; Dubertret, B. *J. Am. Chem. Soc.* **2011**, *133*, 3070−3077.
(44) Ithurria, S.; Dubertret, B. *J. Am. Chem. Soc.* **2008**, *130*, 16504−16505.
(45) Li, Z.; Qin, H. Y.; Guzun, D.; Benamara, M.; Salamo, G.; Peng, X. G. *Nano Res.* **2012**, *5*, 337−351.
(46) Liu, Y. H.; Wang, F. D.; Wang, Y. Y.; Gibbons, P. C.; Buhro, W. E. *J. Am. Chem. Soc.* **2011**, *133*, 17005−17013.